Journal of Polymers and the Environment (2022) 30:308–318
https://doi.org/10.1007/s10924-021-02193-4

ORIGINAL PAPER

A New Montmorillonite-Based Porous Composites: Effectively Removal of Cr(III)-Organic Complexes in Tannery Wastewater

Xin Hao[1] · Tao E[1,2] · Shuyi Yang[1] · Yun Li[3]

Accepted: 25 May 2021 / Published online: 4 June 2021

Abstract

Montmorillonite-based porous adsorbent prepared by gel casting method was used to adsorb Cr(III)-organic complexes in tanning wastewater,together with the initial concentration of 10 mg L^{-1}. The as-porous adsorbent exhibited an excellent performance of separation. Meanwhile, its structural and morphology were characterized by TG, BET, XRD, SEM, EDS and XPS, showing that the porous adsorbent was complete hollow ball structure. And the adsorption results showed that the adsorption amount of porous adsorbent rapidly declined from 9.58 to 5.28 mg L^{-1}, and only Cr(III) was adsorbed, when the molar ratio of Cr(III) and citrate was more than 1:5. Increased of pH was beneficial to adsorb Cr(III)-citrate in range from 2.46 to 7.12. Furthermore, the best removal efficiency of Cr(III)-organic complex was up to 97% and still above 84% after five cycles with porous adsorbent. Finally, the mechanism on adsorbing Cr(III) with porous adsorbent is also provided. Therefore, a kind of porous adsorbent which was easily separated, was prepared to deeply treat tanning wastewater containing Cr(III)-organic complex, and solve the problem of difficult recycle.

Keywords Zirconium oxide · Montmorillonite · Porous adsorbent · Cr(III)-organic complex · Adsorption · Wastewater

Introduction

Tanning industry plays an important role in developing countries [1], and chromium(III) sulfate ($Cr(OH)SO_4 \bullet nH_2O$) has always been considered to be the most effective tanning agent [2]. Metallic chromium (Cr) is mainly discharged from the tanning, retanning and washing stages of leather. However, Cr(III) intake is associated with chronic diseases such as cardiovascular disease, diabetes, and neurological diseases [3–6], and Cr(VI) is even more toxic [7]. Therefore, it is urged to eliminate it from wastewater before discharging to the environment. At present, a rich array of approaches including alkali precipitation [8], photocatalytic degradation [9], membrane filtration [10] and adsorption [11, 12] have been developed to remove Cr(III) from tanning wastewater and Cr(III) can be readily precipitated in alkaline solution [13]. However, the concentration of chromium in the supernatant undergoing alkali precipitation is usually failed to meet the value of 1.5 mg L^{-1} proposed by Chinese environmental protection agency (EPA) [14]. The primary contributor is that a large amount of chemicals, such as organic acids, organic additives, macromolecular organics, collagen hydrolysis macromolecule (– COOH and –OH), are added during the tanning process [15]. Moreover, these organics can coordinate with Cr(III) to form a linear, network-like stable chromium-organic complex through adsorption, charge attraction, and complexation reactions [16]. Compared with other methods, adsorption is a more economical and efficient method to remove chromium from wastewater and thus it is widely used following alkali precipitation [17].

Nowadays, activated carbons, chitosan, natural zeolites and clay minerals are normally applied to remove heavy metals from wastewater [18–21]. Due to its higher adsorption efficiency and larger interlayer cation exchange capacities, richer extensive sources and lower cost, montmorillonite (MMT) is considered to be an important adsorbent to remove heavy metals from wastewater [22, 23]. MMT

✉ Shuyi Yang
yangshuyi@bhu.edu.cn

1 Liaoning Province Crucial Laboratory for Synthesis and Application of Functional Compounds, College of Chemistry and Material Engineering, Bohai University, Jinzhou 121013, Liaoning, China

2 Institute of Ocean Research, Bohai University, Jinzhou 121013, Liaoning, China

3 Chmistry & Chemical Engineering of College Yantai University, Yantai 264005, China

is a yellowish powder with a special 2:1 nanometer layered structure and a large number of cations, as well as selective adsorption properties for Cr(III) [24]. The ideal physical and chemical properties can be used to improve its adsorption performance, mainly contributing by its interlayer cations which are in favor of ion exchange action [25]. Zirconium-based oxides are also regarded as attractive adsorption materials in the field of water treatment, due to its stable, non-toxic and water insoluble properties [26, 27]. Previous researchers have demonstrated that zirconium oxide loaded MMT (ZrO_2-MMT) is feasible and has an excellent adsorption capacity for Cr ions [28]. In most circumstances, the adsorbent is applied in form of powder to treat wastewater. However, the powder is easy to agglomerate in water, resulting in greatly reducing in the specific surface area as well as adsorption capacity. Furthermore, it is difficult to separate powder adsorbent from wastewater, limiting its reusing and recycling. Therefore, it is very valuable to develop a new form of adsorbent to overcome these problems.

Gel casting technique has been used to prepare porous materials, which can effectively support the porous structure before sintering process [29, 30]. Previous reports reveal that the porous adsorbent shows high adsorption capacity, excellent reuse performance and free separation property when removing contaminants from water [23, 30, 31]. Gustafsson et al. [32] studied the mechanisms and modeling of Cr(III) complexation to natural organic matter (NOM). This study suggests that Cr(III)-NOM complexes are important for chromium speciation in many environments. Chen et al. [33] studied tributyl hexadecyl phosphonium solidification strategy to construct gold nanoprobes for the detection of aqueous Cr(III)-organic complexes, and Cr(III)-citrate is selected for the forthcoming study. However, removing Cr(III)-formate and Cr(III)-citrate complexes from tanning wastewater by porous adsorbents is rarely reported.

Herein, the objective of this work is to prepare MMT-based porous adsorbent in method of gel casting, then adsorbing Cr(III)-organic complex in tanning wastewater undergoing alkali precipitation. Formate and citrate are used as organic ligands, exploring the effects of pH, temperature and molar ratio on the adsorption capability of MMT-based porous adsorbent. Since a large number of Na^+ and Ca^{2+} are introduced by alkali precipitation in the tanning wastewater, the effects of interference ions (e.g., Na^+ and Ca^{2+}) are discussed in the adsorption process. Furthermore, industrial wastewater often consists of multiple coexisting anion and cation ions (e.g., Cl^-, SO_4^{2-}, HPO_4^{2-}, Zn(II) and Cr(VI)), and they compete the active adsorption sites with Cr(III). Therefore, the effects of interference ions are also discussed in the adsorption process. In addition, the MMT-based porous adsorbent shows an excellent separation performance and reuse performance during the adsorption-desorption process.

Experimental Details

Preparation of Porous Adsorbent

ZrO_2-MMT composite ($Zr(SO_4)_2$ and MMT in the mass ratio of 3:5) was prepared by ion-exchange method [28]. Acrylamide monomer (12.2 g), *N,N'*-methylenebisacrylamide (MBAM, as cross linker, 1.25 g) and polyacrylic acid salt (as dispersing agent, 1.25 mL) were added to 45 mL of distilled water in condition of stirring. 25 g of ZrO_2-MMT was slowly added to the mixture to form the slurry, together with stirring. Polystyrene ball (as pore-making agent, 115 mL) and triethanolamine dodecyl sulfate (as foamer, 2.5 g) were added to the slurry and stirred for 1 h. Ammonium persulfate (APS, as initiator, 0.0287 g) and *N,N,N',N'*,-tetramethylethylenediamine (TEMED, as catalyst, 0.88 mL) were added to the slurry and stirred for 30 min. Subsequently, the slurry was injected into the mold, drying at 50 °C for 4 h. The temperature was raised from 20 to 380 °C for glue discharge (for 360 min) (Fig. S1). Finally, the dry body was calcinated at temperatures of 600, 700 and 800 °C, for 8 h. An optimum calcination temperature of 600 °C was obtained.

Adsorption Experiments

Adsorption experiments were carried out to evaluate the adsorption performance of the porous adsorbent. The influences of various factors, such as molar ratio (1:0, 1:1, 1:3, 1:5, 1:10, 1:15, 1:20), temperature (20, 40, 60, 80 °C) and pH (2.46, 4.53, 5.45, 6.47, 7.12) on adsorption capacity were examined. A certain amount of organic ligands were added to $Cr_2(SO_4)_3$ solution (10 mg L^{-1}) to prepare Cr(III)-formate and Cr(III)-citrate complex solution. After absorption, the complex solution was filtered through filter membrane.

To evaluate the effect of interfering cations on adsorbing with Cr(III)-citrate (1:5), the porous adsorbent (1 g L^{-1}) was added into Cr(III)-citrate solutions (10 mg L^{-1}) containing 0–25 mmol L^{-1} interfering cations (Na^+ and Ca^{2+}), preparing by dissolving Na_2SO_4 and $CaCl_2$. In the interference experiments, interfering anion ions (10 mg L^{-1}), including Cl^-, SO_4^{2-} and HPO_4^{2-} were added into Cr(III) solutions (10 mg L^{-1}) in form of NaCl, Na_2SO_4 and Na_2HPO_4. In addition, $ZnCl_2$ and $K_2Cr_2O_7$ were used to carry out coexisting cations experiment, which contained 10 mg L^{-1} of Zn(II), Cr(VI) and Cr(III), respectively. Furthermore, 1 M H_2SO_4 or 1 M NaOH solution was used to adjust its pH.

To evaluate the recyclability of the porous adsorbent, five times adsorption-desorption experiments were carried

out. The consumed porous adsorbent was immersed in 0.1 M H_2SO_4 solution and shaken for 24 h. Then the desorbed porous adsorbent was filtrated, washed and dried for the next cycle. Finally, the inductively coupled plasma (ICP) technique (Varian Liberty 200 ICP-OES) was used to measure the concentration of Cr(III) in the solution.

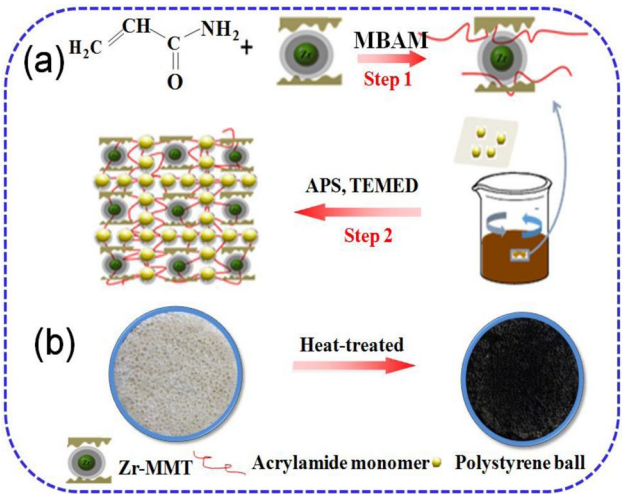

Fig. 1 Schematic illustration of the prepared porous adsorbent: **a** step 1 added Zr-MMT to acrylamide monomer mixture and stirred; step 2 added the polystyrene ball to the slurry and stirred; **b** the slurry was injected into the mold, dried at 50 °C for 4 h, then heat-treated at 600, 700 or 800 °C for 8 h

Results and Discussion

Preparation process of the porous adsorbent

The preparation process of the porous adsorbent is shown in Fig. 1. Briefly, ZrO_2-MMT composite, organic monomers and polystyrene balls are mixed to prepare slurry in the prescribed sequence. Then the injection mold is formed into a wet body, as shown in Fig. 1. Next, the wet body is dried at 50 °C to obtain a dry body. The temperature is raised from 20 to 380 °C (for 360 min) for glue discharge (Fig. S1). Therefore, the position of the polystyrene spheres is released and produced a porous structure after the glue discharge. Finally, the porous adsorbent is obtained after thermal treatment at 600 °C as shown in Fig. 1.

TG, FTIR and XPS Spectra Analysis

Figure 2a presents the TG curves of the MMT and porous adsorbent. The weight loss of MMT is about 7.4% between 35 and 200 °C, which is adsorbed water. And the weight loss is about 2.8% between 200 and 700 °C, which is lattice water. Because the main component of MMT is aluminosilicate, so the thermal stability is good. At the same time, the TG curve of the dry body slowly declines from 35 to 100 °C, mainly due to dehydration of the dry body and the desorption process of adsorbed water molecules between the MMT surface and the layer [34]. Then the mass of dry

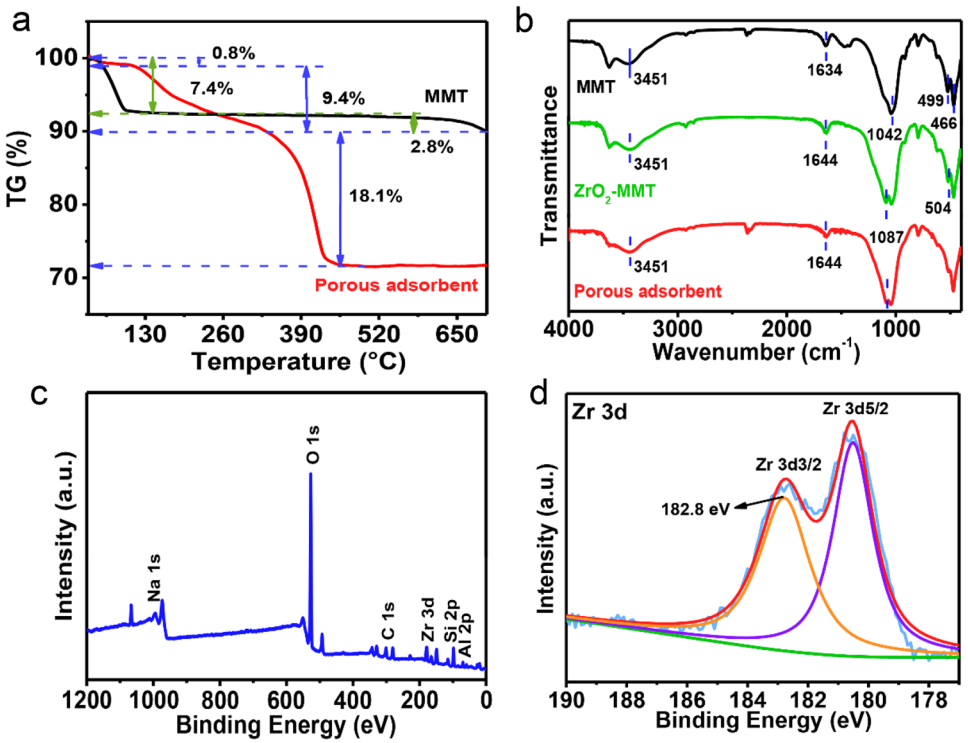

Fig. 2 **a** TG curves of the MMT and porous adsorbent; **b** FTIR spectra of MMT, ZrO_2-MMT and porous adsorbent; **c** XPS survey spectrum of porous adsorbent; **d** high resolution XPS spectrum of Zr 3d

body significantly decreases in the range of 100–330 °C, mainly because of the decomposition of polyacrylamide at 200 °C. When the temperature increases to 300 °C, it decomposes into NH_3, and then it decomposes into H_2, CO and NH_3 above 300 °C. Subsequently, the polystyrene sphere is severely degraded in the range of 330–450 °C. Therefore, the mass loss of the dry body is presumably due to the decomposition of organic substances such as polyacrylamide and polystyrene spheres in the slurry [34].

Figure 2b displays the FTIR spectra of MMT, ZrO_2-MMT and porous adsorbent. For MMT, the peaks at 466, 1042, 1634 and 3451 cm^{-1} are attributed to the vibration of Al–O, stretching vibration of Si–O, bending vibration of H–OH and stretching vibration of O–H, respectively. Compared with MMT, the bands of Si–O–Si in the ZrO_2-MMT shift to 504 cm^{-1}, indicating ZrO_2 enters into the layers structure of MMT [35]. In addition, the FTIR spectra of ZrO_2-MMT and porous adsorbent show an important band at 504 cm^{-1} corresponding to the vibration of the Zr–O bond [36]. Furthermore, compared with the pristine MMT, the XRD spectra of the porous adsorbent show obvious diffraction peaks at 30.50º and 50.58º (Fig. S2), corresponding to the (101) and (211) diffraction planes of ZrO_2, respectively [36, 37]. This result also indicates that ZrO_2 exists in the layer structure of the porous adsorbent. Compared with ZrO_2-MMT, few changes are observed in the FTIR spectrum of porous adsorbent when the powder is prepared as porous material, due to adding carbonized organics.

XPS analysis is used to discuss the chemical and structural information of the porous adsorbent. The full spectra of XPS reveal the existence of elements Zr, Al, Si, C, Na and O (Fig. 2c). The peaks of binding energy (182.8 eV) can be assigned to Zr 3d (Fig. 2d), indicating the existence of ZrO_2.

SEM-EDS and BET analysis

The morphological feature of porous adsorbent is shown in Fig. 3. Subjecting to thermal treatment at 600 °C, there is a hollow sphere structure inside the porous adsorbent, forming an integral pore structure (Fig. 3a and b). The wall of the porous adsorbent is observed in Fig. 3c and d, and it is in a clear porous structure with certain interlayer spacing as well as a smooth surface. With the increase of temperature, the pore structure becomes not integral (Fig. S3). The wrinkled layered structure of the spherical wall section is clearly presented in Fig. 3e and f. The thickness of the wall is about 12–20 µm, suggesting that the layer structure of MMT in porous adsorbent remains integral.

The data on specific surface area, pore size and pore volume of MMT, ZrO_2-MMT and porous adsorbent, is listed in Table S1. The specific surface area of the porous adsorbent (38.80 $m^2\ g^{-1}$) is almost equivalent to that of ZrO_2-MMT (40.56 $m^2\ g^{-1}$), indicating that the gel casting

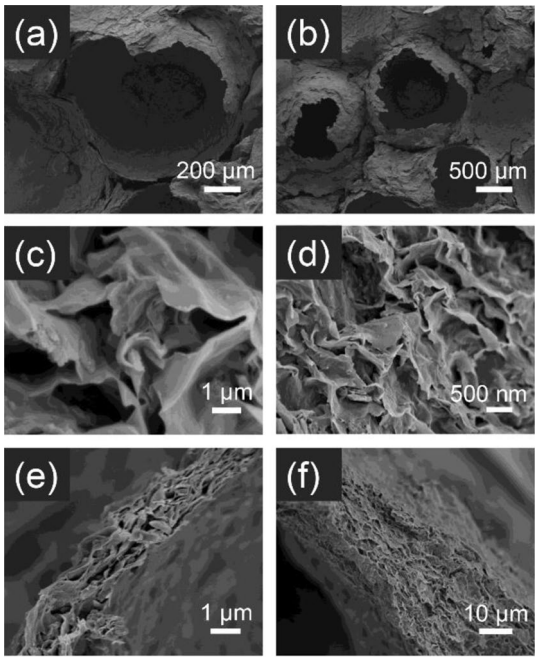

Fig. 3 SEM images of the: **a** and **b** hollow sphere structure, scale bar = 200 and 500 µm; **c** and **d** wall, scale bar = 1 µm and 500 nm; **e** and **f** spherical wall section, scale bar = 1 and 10 µm

method is feasible for ZrO_2-MMT molding. In addition, the value of pore size (13.93 nm) also proves the existence of mesoporous. The pore volumes of MMT and ZrO_2-MMT are 0.0048 and 0.0028 $cm^3\ g^{-1}$, respectively. The reduced pore volume is probably caused by the existence of ZrO_2 in the MMT sheet, proving that ZrO_2 has entered into the layers of MMT.

Adsorption Experiments

As shown in Fig. 4a, the adsorption amount of the porous adsorbent is not serious changed with increasing molar ratio of formate and Cr(III), which indicates that formate plays a less important role in the process. With a changed molar ratio of Cr(III) and citrate ranging from 1:1 to 1:5, the adsorption amount of Cr(III)-citrate is not corresponding changed. This result can be attributed to strong positively charged, causing by the existing of Cr(III) in form of $Cr(H_2O)_6^{3+}$ in an aqueous solution [38]. While the adsorption amount of Cr(III)-citrate rapidly declined when the mole ratio of Cr(III) and citrate is more than 1:5. Since there are three carboxyl groups in its molecular structure, citrate has the stronger coordination function for Cr(III). In the adsorption process, the movement of Cr(III) is restricted by citrate, and they are positive proportion relation. Since there are three carboxyl groups in its molecular structure. Furthermore, the complexation reaction of Cr^{3+} with citric acid is as follows:

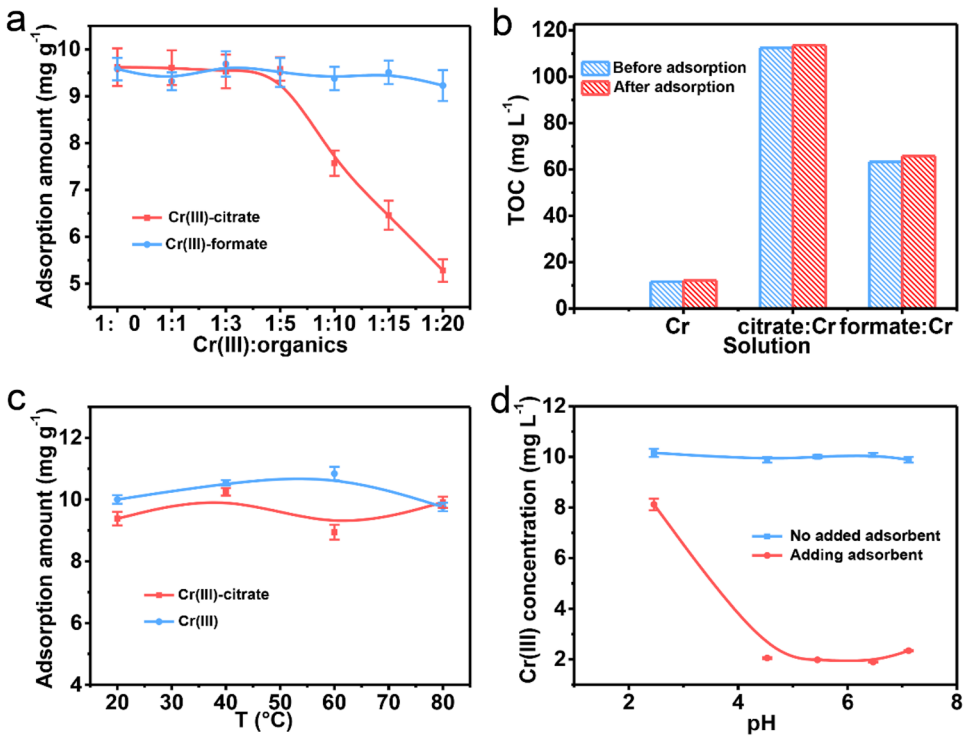

Fig. 4 **a** The effect of molar ratio of organics and Cr(III); **b** TOC changes of Cr(III)-organic complex adsorbed on porous adsorbent; **c** The adsorption curves of Cr(III)-citrate and Cr(III) on the porous adsorbent at various temperatures; **d** The effect of pH on the concentration of Cr(III) in Cr(III)-citrate solution before and after addition adsorbent (adsorbent dose = 1 g L^{-1}; adsorption time = 60 min)

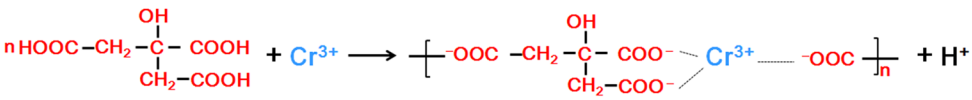

(1)

When the molar ratio of citrate and Cr(III) increases, the equilibrium shifts to the form of the complex, resulting a decreased concentration of Cr(III) in the solution, as well as decreasing the amount of Cr(III) being adsorbed.

To explore the adsorption performance of the adsorbent for organic ligands, then total organic carbon (TOC) is employed to measure total carbon of organic ligands in solution before and after adsorption. There is no external carbon source before and after adsorbing of Cr(III)-organic complexes on porous adsorbent. As can be seen from Fig. 4b, there is no change in the amount of TOC before and after adsorption. The result reveals that the porous adsorbent adsorbs Cr(III), whereby organic ligands are not adsorbed, further illustrating that the increased organic ligands can restrict the movement of Cr(III) and impair the adsorption amount of porous adsorbent.

The adsorption curves of the porous adsorbent at various temperatures are depicted in Fig. 4c. With the increased temperature, the adsorption amount of Cr(III)-citrate is not regularly changed. It can be explained that the carboxyl group in the molecular structure of citrate plays more important role in forming Cr(III) than the force generated by the thermal motion on Cr(III). With the increasing temperature, the adsorption amount of Cr(III) alone slightly increases followed by gradually decreasing, which is mainly due to the fact that valency forces of Cr(III) in the solution becomes stronger. It is beneficial for Cr(III) to overcome the electrostatic repulsion and space hindrance during the adsorption process. As a result, the numbers of active site with porous adsorbent are increased, which is in favor of Cr(III) combination. However, the adsorption amount of Cr(III) on the porous adsorbent decreases, it can be attributed to more intensely moved Cr(III) as well as partially desorbed Cr(III).

The concentration of Cr(III) in the Cr(III)-citrate system is basically about 10 mg L^{-1} without adding adsorbent (Fig. 4d). With increasing pH, the concentration of Cr(III)-citrate significantly decreases after adding adsorbent. It is explained that the increased pH impairs the complexation force between citrate and Cr(III). When pH is in range from 4.53 to 7.12, the residual concentration of Cr(III) is slightly changed. It may be due to the fact that the adsorbed Cr(III) is not able to desorb at higher pH. The as-prepared porous adsorbent obtains complete hollow ball structure and large specific surface area, which is beneficial for adsorbing Cr(III)-citrate at high pH. In addition, zeta potential of the porous adsorbent is negatively charged with pH in the range

from 2.89 to 11.22, in favor of adsorbing of positive charged heavy metals.

Influence of interfering ions and reusability of the porous adsorbent

Various coexisting cations in the tanning wastewater interferes the adsorption amount of porous adsorbent for Cr(III)-citrate. Na^+ and Ca^{2+} are used as interfering cations to investigate their effects on adsorbing Cr(III)-citrate (Fig. 5a). Na^+ and Ca^{2+} can interfere the up taking Cr(III)-citrate, mainly due to the fact that Na^+ and Ca^{2+} compete active adsorption sites with Cr(III). Figure 5b shows that the adsorption amount is not significantly inhibited in the presence of these competing anions (Cl^-, SO_4^{2-}), except for HPO_4^{2-} ion. The result is mainly due to the similar tetrahedral structure of chromium and phosphate. Figure 5c shows Cr(III) is effectively removed with the porous adsorbent, but it performs low adsorption efficiency for other metal ions, such as Zn(II) and Cr(VI).

Figure 5d depicts that the change of adsorption capacity of the porous adsorbent in five times adsorption-desorption cycles. The removal efficiency of five times adsorption-desorption cycles is 97%, 95%, 91%, 89 and 84%, respectively. The results show that the removal efficiency of the porous adsorbent for Cr(III)-citrate decreases from 97 to 84% as time going, suggesting that porous adsorbent has good stability and reusability. Furthermore, the porous adsorbent is easier to separate from the effluent than powder, and do not produce secondary pollution (Fig. S4).

The adsorbed porous adsorbent is immersed in 1 M H_2SO_4 solution and shaken for 24 h. Then, 0.1 M H_2SO_4 or 0.1 M NaOH solution is used to adjust pH value (2–3). The hydrolysis formula of chromium is as follows [39]:

$$7[Cr(H_2O)6]^{3+} \rightleftharpoons [Cr(H_2O)6OH]^{2+} + 29H_2O + Cr_2(OH)^{24+} + Cr_3(OH)^{45+} + Cr^{3+} + 7H^+ \quad (2)$$

According to the requirement, desorption solution of chromium is prepared with different acidity and alkalinity, which is reused for leather tanning. This process realizes the function reuse of waste and has a good economic value in industrial production.

Adsorption Mechanism

Adsorption Kinetic

$$log(q_e - q_t) = logq_e - \frac{k_1}{2.303}t \quad (3)$$

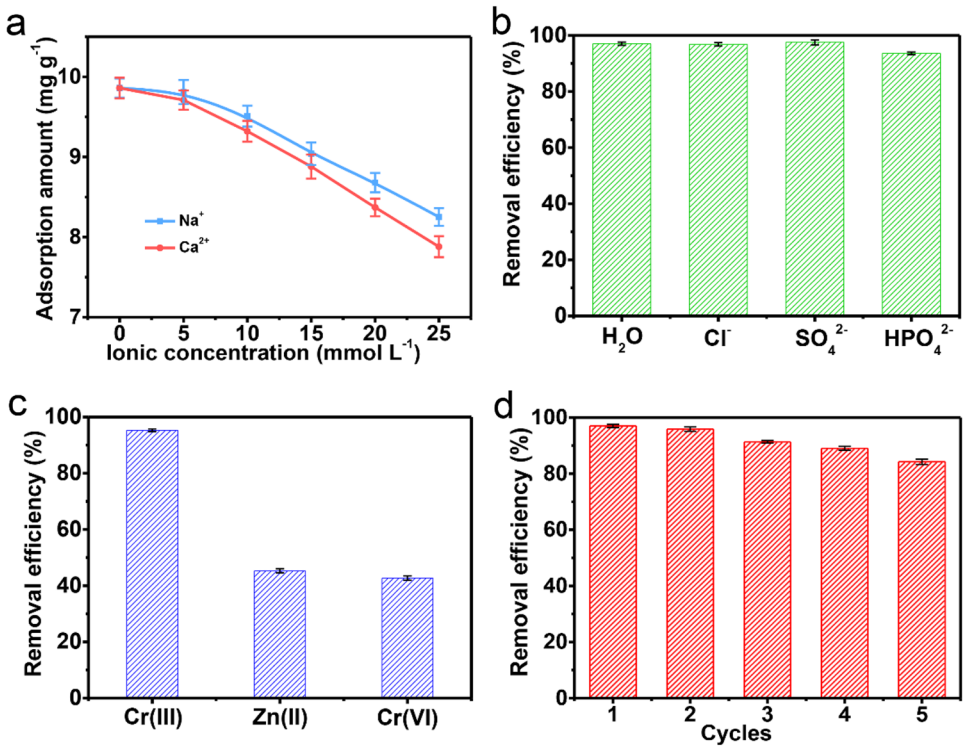

Fig. 5 **a** Effect of competing cations (Na^+ and Ca^{2+}) on adsorbing Cr(III)-citrate with porous adsorbent (adsorbent dose = 1 g L^{-1}; C_0 = 10 mg L^{-1}; adsorption time = 60 min; pH 6.5); **b** Effects of the coexisting anions and the **c** coexisting cations on adsorbing Cr(III); **d** Recycling of porous adsorbent (adsorbent dose = 1 g L^{-1}; C_0 = 10 mg L^{-1}; adsorption time = 60 min; pH 6.5)

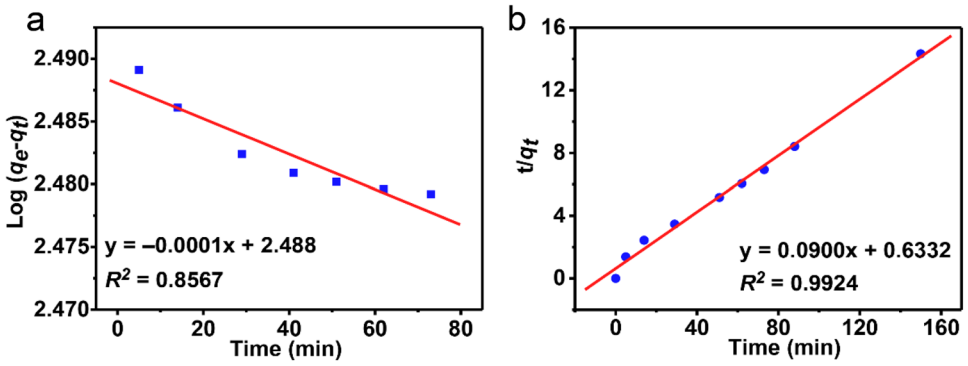

Fig. 6 The kinetic adsorption data plots for adsorbing Cr(III) on the porous adsorbent **a** pseudo-first-order equation and **b** pseudo-second-order equation

Table 1 The first-order, second-order kinetic parameters on adsorbing Cr(III) with porous adsorbent

Kinetic model	Parameters	Porous adsorbent
first-order kinetic	k_1 ($\times 10^{-3}$)	0.23 ± 0
	q_e (mg g^{-1})	307.61 ± 0.28
	R^2	0.8567 ± 0.0407
s-order kinetic	k_2 ($\times 10^{-3}$)	12.69 ± 6.89
	q_e (mg g^{-1})	11.11 ± 1.74
	R^2	0.9924 ± 0.0044

In order to explore the adsorption behavior of Cr(III) on the porous adsorbent, the data on Cr(III) adsorption is fitted using the Pseudo-first-order and Pseudo-second-order kinetic equations:

$$\frac{t}{q_t} = \frac{1}{q_e}t + \frac{1}{k_2 q_e^2} \tag{4}$$

where t is the adsorption time (min); q_e represents the adsorption amount of porous adsorbent for Cr(III) at equilibrium adsorption (mg g^{-1}); k_1 (min^{-1}) and k_2 (g mg^{-1} min^{-1}) represent the rate constants of the Pseudo-first-order and Pseudo-second-order kinetic models.

As shown in Fig. S5a, when the time reaches 70 min, the adsorption equilibrium of Cr(III) on porous adsorbent is established. The fitting parameters are exhibited in Table 1. The adsorption data fittings of kinetic models of Cr(III) on porous adsorbent are showed in Fig. 6a and b. The R^2 ($R^2 = 0.9924$) value of pseudo-second-order kinetic model is much higher than that of the pseudo-first-order kinetic model ($R^2 = 0.8567$). Further, the calculated value of pseudo-second-order kinetic equation is 11.11 mg g^{-1}, which is closer to the experimental value of 10.46 mg g^{-1}. Therefore, the pseudo-second-order kinetic equation can better fit the adsorption process, which reveals that the adsorption process is mainly chemical adsorption.

Adsorption isotherm

In order to evaluate the mechanism on adsorbing Cr(III) with porous adsorbent, the adsorption data is fitted by the linear forms of the Langmuir and Freundlich isotherm models as follows:

$$\frac{C_e}{q_e} = \frac{1}{q_m b} + \frac{C_e}{q_m} \tag{5}$$

$$logq_e = \frac{1}{n}logC_e + logk \tag{6}$$

where b is the Langmuir constant, (L mg^{-1}); q_m represents the maximum adsorption capacity of porous adsorbent, (mg g^{-1}); C_e is the concentration of Cr(III) at equilibrium adsorption, (mg L^{-1}); k and n represent the Freundlich constants.

Figure S5b shows the effect of the initial concentration of Cr(III). The values of fitting parameters are exhibited

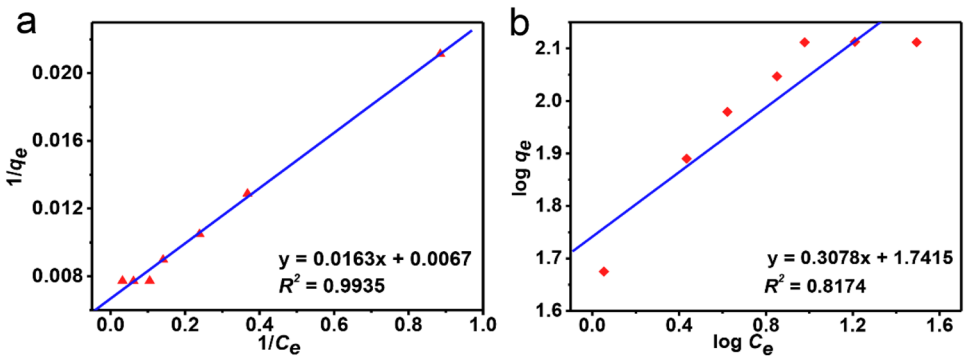

Fig. 7 Linear regression fitting of the adsorption data on Cr(III) with the porous adsorbent using (a) Langmuir equation and (b) Freundlich equation

Table 2 The adsorption isotherm parameters on adsorbing Cr(III) with porous adsorbent

Isotherm model	Parameters	Porous adsorbent
Langmuir	q_e (mg g^{-1})	129.63 ± 2.0
	q_m (mg g^{-1})	149.25 ± 2.27
	R^2	0.9935 ± 0.0007
Freundlich	K [$1^{1/n}$/(mg$^{1-1/n}$g)]	55.14 ± 1.42
	n	3.25 ± 0.04
	R^2	0.8174 ± 0.0338

in Table 2. The linear data fittings by the isotherm models are shown in Fig. 7a and b. The experimental data agrees well with both Langmuir ($R^2 = 0.9935$) and Freundlich ($R^2 = 0.8174$) models, the theoretical maximum adsorption capacity q_m (149.25 mg g^{-1}) is closer to the equilibrium adsorption amount q_e (129.63 mg g^{-1}). Therefore, the Langmuir isotherm model can appropriately describe the adsorption process. Accordingly, the adsorption process of porous adsorbent for Cr(III) is mainly monolayer adsorption. The value of n is the adsorption strength. The good adsorption property of porous adsorbent is proved by the value of $n = 3.25$ (between 1 and 10).

Thermodynamics

XPS, Zeta and EDS Analysis

As shown in Fig. 8a, the peak of Cr element appears after adsorbing Cr(III), which illustrated that Cr(III) has been adsorbed by porous adsorbent [40, 41]. In addition, in the high-resolution spectrum of Cr 2p, the peaks of binding energy (575.2 eV) of Cr 2p appear after adsorption (Fig. 8b), which corresponds to Cr(III), indicating that the porous adsorbent has adsorption capacity to Cr(III) [42, 43]. Therefore, the valence state of Cr(III)-organic complexes did not change before and after adsorption. Additionally, the zeta potential of MMT and porous adsorbent at different pH is depicted in Fig. 8c. The zeta potential of the porous adsorbent is negatively charged with pH in the range of 2.89–11.22, which is beneficial to adsorb heavy metals in solutions.

Figure 8d and e show the SEM images before and after adsorbing Cr(III)-organic complexes with the porous adsorbent. It can be seen that the layer surface of the porous adsorbent is smooth and clear in Fig. 8d. The surface of the porous adsorbent appears fragments and becomes relatively rough after adsorption (Fig. 8e), indicating that the porous adsorbent has an adsorption capacity to Cr(III). In addition, the result of adsorbing Cr(III) ions is also confirmed by EDS analysis (insets in Fig. 8d and e). Fig. S7b clearly shows the presence of Cr element after adsorption. It also proves that Cr(III) has been adsorbed by porous adsorbent.

Comparisons of Adsorption Capacity of Various Adsorbents to Cr(III)

The comparison of the maximum adsorption capacity to Cr(III) on various adsorbents reported in the literature are listed in Table 4 [16, 44–48]. As shown in Table 4, the adsorption capacity of this porous adsorbent is the largest and outperforms many other adsorbents. To sum up, montmorillonite-based porous composites not only show good adsorption performance, but also separate easily, which will not cause secondary pollution.

Conclusions

In summary, montmorillonite-based porous adsorbent is successfully prepared via gel casting method. The adsorbent is characterized by TG, BET, XRD, SEM, EDS and XPS. The results indicate that the gelatinization temperature of dry body is 380 °C, and the specific surface area of porous adsorbent is basically consistent with that of pristine MMT. If the calcination temperature is 600 °C, the pore structure in the porous material is complete, for the pore wall and section lamellar structure are clear, and the pore channel can be seen, and the adsorption performance is the best. In addition, adsorption test results show that the performance of the adsorbent is significantly influenced, when the molar ratio

Table 3 The adsorption thermodynamic parameters on adsorbing Cr(III) with porous adsorbent

T(K)	b	K_a	ΔH (kJ mol^{-1})	ΔS (kJ mol^{-1})	ΔG (kJ mol^{-1})
333	0.41 ± 0.01	61.35 ± 2.34	6.57 ± 0.002	0.05 ± 0.002	-10.78 ± 0.71

The relevant parameters are presented in Table 3. Plot of ln *Ka* versus 1000/T is shown in Fig. S6. The positive value of ΔH reflects the fact that adsorption of Cr(III) on porous adsorbent is an endothermic process. The negative value of ΔG implies the feasibility and spontaneity of adsorbing Cr(III) on the surface of porous adsorbent. During the adsorption process, the increased randomness of the system solid/solution interface is shown by the positive values of ΔS. This result indicates that porous adsorbent has high affinity to Cr(III)

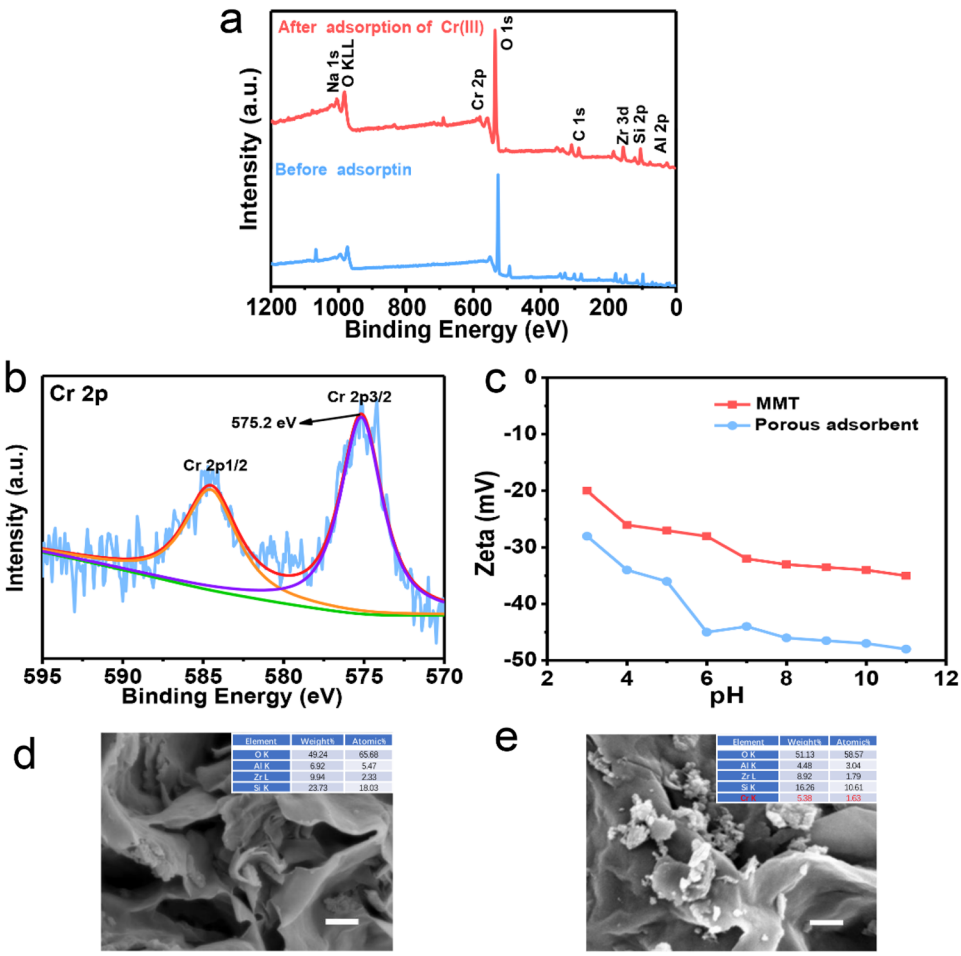

Fig. 8 **a** XPS survey spectra of porous adsorbent before and after adsorbing Cr(III); **b** high resolution XPS spectrum of Cr 2p; **c** Zeta potential of MMT and porous adsorbent with different pH values; SEM images and EDS analysis (insets) of porous adsorbent: **d** before adsorbing Cr(III), scale bar = 200 nm and **e** after adsorbing Cr(III), scale bar = 200 nm

Table 4 Maximum adsorption capacity (q_m) to Cr(III) by with various adsorbents in other reports

Adsorbents	q_m (mg g^{-1})	References
Humic acid modified Ca-montmorillonite	15.66	[44]
Silica/sulfonate (SFS)	72.8	[45]
Corncob waste activated carbon	84.55	[46]
MAC-pseudo-non-imprinted adsorbent	69.61	[47]
Gelatin-Montmorillonite Nanocomposite	52.91	[16]
Fe_3O_4–SiO_2 sub-micron particles	9.00 ± 3.00	[48]
Porous adsorbent	149.25	This work

of Cr(III) and citrate is greater than 1:5. Temperature plays no evident role during the adsorption process. Increased pH is beneficial to adsorb Cr(III)-citrate as pH rises from 2.46 to 7.12. The pseudo-second-order kinetic equation and the Langmuir isotherm equation can better describe the adsorption process. In terms of adsorbing Cr(III), the porous adsorbent is superior to many other adsorbents. The removal efficiency decreases from 97 to 84% after five adsorption-desorption cycles when the concentration of Cr(III)-citrate is 10 mg L^{-1}. Our results exhibit that montmorillonite-based porous adsorbent has an excellent reuse performance and easily separating property in the adsorption process, which can deeply treat tanning wastewater undergoing alkali precipitation. Finally, the adsorption mechanism reveals that electrostatic attraction may contribute to the adsorption of Cr(III). The results of EDS and XPS analysis reveal that Cr(III) is adsorbed on the porous adsorbent. Therefore, montmorillonite-based porous adsorbent is a promising material for removing Cr(III)-organic complex from tanning wastewater with low concentration (10 mg L^{-1}).

Supplementary Information.

The analytical methods of montmorillonite-based porous composites are available in the supplementary information. The thermal treatment flow chart of the adsorbent is shown in Fig. S1. XRD patterns of pristine MMT and porous adsorbent are shown in Fig. S2. SEM images of the hollow sphere structure at 700 and 800 °C are shown in Fig. S3. Easily separable process of adsorbed porous adsorbent is shown in Fig. S4. The effect of time (adsorbent dose = 1 g L^{-1}; C_0 = 10 mg L^{-1}) and initial Cr(III) concentration (adsorbent dose = 1 g L^{-1}; adsorption time = 60 min; C_0 = 50–160 mg L^{-1}) on

Cr(III) adsorption are shown in Fig. S5a and b. Plot of ln *Ka* versus 1000/T for Cr(III) adsorption on porous adsorbent is shown in Fig. S6. EDS spectra of adsorbent before and after adsorbing Cr(III) are shown in Fig. S7. Specific surface area, pore size and pore volume of MMT, Zr-MMT and porous adsorbent are listed in Table S1.

Supplementary Information The online version of this article (https://doi.org/10.1007/s10924-021-02193-4) contains supplementary material, which is available to authorized users.

Acknowledgements The research was supported by Liaoning Province (Jinzhou) Fur Green Manufacturing Industry Technology Innovation Strategic Alliance [201854], Research on resource recycling technology of tanned chromium-containing waste dander [2018020190-301], The "Seedling" Project named "Research on Graphene-based 3D Material Construction and Key Technologies for Industrialization Application" for Youth Science and Technology Talents of Education Department of Liaoning Province (LQ2020011), Study on the deep removal of heavy metal chromium from industrial wastewater in the upper reaches of Daling River estuary [BDHYYJY2020013] (This study were supported by the Open Fund of Institute of Ocean Research, Bohai University), National Natural Science Foundation of China [21878024], Innovation Team Project of Liaoning Province [LT2015001], and Innovation Team Project of Liaoning Higher University [2018479-14].

Data availability The datasets used and/or analyzed during the current study are available from the corresponding author on reasonable request.

Declarations

Conflict of interest We declare that we have no financial and personal relationships with other people or organizations that can inappropriately influence our work, there is no professional or other personal interest of any nature or kind in any product, service or company. No conflict of interest exits in the submission of this manuscript, and manuscript is approved by all authors for publication. I would like to declare on behalf of my co-authors that the work described was original research that has not been published previously, and not under consideration for publication elsewhere, in whole or in part.

Conflict of interest The authors declare that they have no conflict of interest.

References

1. Lofrano G, Meric S, Zengin GE, Orhon D (2013) Chemical and biological treatment technologies for leather tannery chemicals and wastewaters: a review. Sci Total Environ 461–462:265–281. https://doi.org/10.1016/j.scitotenv.2013.05.004
2. Covington AD (1997) Modern tanning chemistry. Chem Soc Rev 26:111. https://pubs.rsc.org/en/content/articlehtml/1997/cs/cs9972600111
3. He X, Wu C, Qian Y, Li Y, Zhang L, Ding F, Chen H, Shen J (2019) Highly sensitive and selective light-up fluorescent probe for monitoring gallium and chromium ions in vitro and in vivo. Analyst 144:3807–3816. https://doi.org/10.1039/c9an00625g
4. He X, Chen H, Xu C, Fan J, Xu W, Li Y, Deng H, Shen J (2020) Ratiometric and colorimetric fluorescent probe for hypochlorite monitor and application for bioimaging in living cells, bacteria and zebrafish. J Hazard Mater. https://doi.org/10.1016/j.jhazmat.2020.122029
5. He X, Deng Z, Xu W, Li Y, Xu C, Chen H, Shen J (2020) A novel dual-response chemosensor for bioimaging of exogenous/endogenous hypochlorite and hydrazine in living cells, pseudomonas aeruginosa and zebrafish. Sens Actuators B. https://doi.org/10.1016/j.snb.2020.128450
6. He X, Xu C, Xiong W, Qian Y, Fan J, Ding F, Deng H, Chen H, Shen J (2019) The ICT-based fluorescence and colorimetric dual sensing of endogenous hypochlorite in living cells, bacteria, and zebrafish. Analyst 145:29–33. https://doi.org/10.1039/c9an02226k
7. Hokkanen S, Bhatnagar A, Repo E, Lou S, Sillanpää M (2016) Calcium hydroxyapatite microfibrillated cellulose composite as a potential adsorbent for the removal of Cr(VI) from aqueous solution. Chem Eng J 283:445–452. https://doi.org/10.1016/j.cej.2015.07.035
8. Meunier N, Drogui P, Montane C, Hausler R, Mercier G, Blais JF (2006) Comparison between electrocoagulation and chemical precipitation for metals removal from acidic soil leachate. J Hazard Mater 137:581–590. https://doi.org/10.1016/j.jhazmat.2006.02.050
9. Yang Y, Wang G, Deng Q, Ng DH, Zhao H (2014) Microwave-assisted fabrication of nanoparticulate TiO_2 microspheres for synergistic photocatalytic removal of Cr(VI) and methyl orange. ACS Appl Mater Inter 6:3008–3015. https://doi.org/10.1021/am405607h
10. Religa P, Kowalik A, Gierycz P (2011) Application of nanofiltration for chromium concentration in the tannery wastewater. J Hazard Mater 186:288–292. https://doi.org/10.1016/j.jhazmat.2010.10.112
11. Wang D, Zhang G, Dai Z, Zhou L, Bian P, Zheng K, Wu Z, Cai D (2018) Sandwich-like nanosystem for simultaneous removal of Cr(VI) and Cd(II) from water and soil. ACS Appl Mater Inter 10:18316–18326. https://doi.org/10.1021/acsami.8b03379
12. Elabbas S, Mandi L, Berrekhis F, Pons MN, Leclerc JP, Ouazzani N (2016) Removal of Cr(III) from chrome tanning wastewater by adsorption using two natural carbonaceous materials: eggshell and powdered marble. J Environ Manage 166:589–595. https://doi.org/10.1016/j.jenvman.2015.11.012
13. Liu J, Huang K, Xie K, Yang Y, Liu H (2016) An ecological new approach for treating Cr(VI)-containing industrial wastewater: photochemical reduction. Water Res 93:187–194. https://doi.org/10.1016/j.watres.2016.02.025
14. Ye Y, Jiang Z, Xu Z, Zhang X, Wang D, Lv L, Pan B (2017) Efficient removal of Cr(III)-organic complexes from water using UV/Fe(III) system: negligible Cr(VI) accumulation and mechanism. Water Res 126:172–178. https://doi.org/10.1016/j.watres.2017.09.021
15. Wang D, Ye Y, Liu H, Ma H, Zhang W (2018) Effect of alkaline precipitation on Cr species of Cr(III)-bearing complexes typically used in the tannery industry. Chemosphere 193:42–49. https://doi.org/10.1016/j.chemosphere.2017.11.006
16. Qiu J, Dong S, Wang H, Cheng X, Du Z (2015) Adsorption performance of low-cost gelatin–montmorillonite nanocomposite for Cr(III) ions. RSC Adv 5:58284–58291. https://pubs.rsc.org/en/content/articlepdf/2015/ra/c5ra08781c
17. Ijagbemi CO, Baek MH, Kim DS (2009) Montmorillonite surface properties and sorption characteristics for heavy metal removal from aqueous solutions. J Hazard Mater 166:538–546. https://doi.org/10.1016/j.jhazmat.2008.11.085
18. Dong Z, Zhang F, Wang D, Liu X, Jin J (2015) Polydopamine-mediated surface-functionalization of graphene oxide for heavy metal ions removal. J Solid State Chem 224:88–93. https://doi.org/10.1016/j.jssc.2014.06.030
19. Abou-El-Sherbini KS, Hassanien MM (2010) Study of organically-modified montmorillonite clay for the removal of copper(II).

J Hazard Mater 184:654–661. https://doi.org/10.1016/j.jhazmat.2010.08.088
20. Di Natale F, Erto A, Lancia A, Musmarra D (2015) Equilibrium and dynamic study on hexavalent chromium adsorption onto activated carbon. J Hazard Mater 281:47–55. https://doi.org/10.1016/j.jhazmat.2014.07.072
21. Gong K, Hu Q, Yao L, Li M, Sun D, Shao Q, Qiu B, Guo Z (2018) Ultrasonic pretreated sludge derived stable magnetic active carbon for Cr(VI) removal from wastewater. ACS Sustainable Chem Eng 6:7283–7291. https://doi.org/10.1021/acssuschemeng.7b04421
22. Yu P, Wang H-Q, Bao R-Y, Liu Z, Yang W, Xie B-H, Yang M-B (2017) Self-assembled sponge-like chitosan/reduced graphene oxide/montmorillonite composite hydrogels without cross-linking of chitosan for effective Cr(VI) sorption. ACS Sustainable Chem Eng 5:1557–1566. https://doi.org/10.1021/acssuschemeng.6b02254
23. Cheng W, Ding C, Nie X, Duan T, Ding R (2017) Fabrication of 3D macroscopic graphene oxide composites supported by montmorillonite for efficient U(VI) wastewater purification. ACS Sustainable Chem Eng 5:5503–5511. https://doi.org/10.1021/acssuschemeng.7b00841
24. Zhu J, Cozzolino V, Pigna M, Huang Q, Caporale AG, Violante A (2011) Sorption of Cu, Pb and Cr on Na-montmorillonite: competition and effect of major elements. Chemosphere 84:484–489. https://doi.org/10.1016/j.chemosphere.2011.03.020
25. Jin J, Xiao T, Tan Y, Zheng J, Liu R, Qian G, Wei H, Zhang J (2018) Effects of TiO_2 pillared montmorillonite nanocomposites on the properties of asphalt with exhaust catalytic capacity. J Clean Prod 205:339–349. https://doi.org/10.1016/j.jclepro.2018.08.251
26. Dou X, Mohan D, Pittman CU, Yang S (2012) Remediating fluoride from water using hydrous zirconium oxide. Chem Eng J 198–199:236–245. https://doi.org/10.1016/j.cej.2012.05.084
27. Reddy CV, Babu B, Reddy IN, Shim J (2018) Synthesis and characterization of pure tetragonal ZrO_2 nanoparticles with enhanced photocatalytic activity. Ceram Int 44:6940–6948. https://doi.org/10.1016/j.ceramint.2018.01.123
28. Ma ET, Yang D, Sun S, Xu Y, Kim J EJ (2019) Zirconium dioxide loaded montmorillonite composites as high-efficient adsorbents for the removal of Cr^{3+} ions from tanning wastewater. J Solid State Chem 277:502–509. https://doi.org/10.1016/j.jssc.2019.07.002
29. Zhang F-Z, Kato T, Fuji M, Takahashi M (2006) Gelcasting fabrication of porous ceramics using a continuous process. J Eur Ceram Soc 26:667–671. https://doi.org/10.1016/j.jeurceramsoc.2005.07.021
30. Li ET, Yang Y, Qian S, Liu J, Xing L J (2018) Nano-montmorillonite-based porous material prepared by gel casting: structure and adsorption properties. Micro Nano Lett 13:332–334. https://doi.org/10.1049/mnl.2017.0531
31. Alsbaiee A, Smith BJ, Xiao L, Ling Y, Helbling DE, Dichtel WR (2016) Rapid removal of organic micropollutants from water by a porous beta-cyclodextrin polymer. Nature 529:190–194. https://doi.org/10.1038/nature16185
32. Gustafsson JP, Persson I, Oromieh AG, van Schaik JW, Sjostedt C, Kleja DB (2014) Chromium(III) complexation to natural organic matter: mechanisms and modeling. Environ Sci Technol 48:1753–1761. https://doi.org/10.1021/es404557e
33. Chen N, Pan B (2021) Tributylhexadecylphosphonium modification strategy to construct gold nanoprobes for the detection of aqueous Cr(III)-organic complexes. Anal Chem 93:1811–1817. https://doi.org/10.1021/acs.analchem.0c04688
34. Zhu L, Wang L, Xu Y (2017) Chitosan and surfactant co-modified montmorillonite: a multifunctional adsorbent for contaminant removal. Appl Clay Sci 146:35–42. https://doi.org/10.1016/j.clay.2017.05.027
35. Zhang G, He Z, Xu W (2012) A low-cost and high efficient zirconium-modified-Na-attapulgite adsorbent for fluoride removal from aqueous solutions. Chem Eng J 183:315–324. https://doi.org/10.1016/j.cej.2011.12.085
36. Saha I, Ghosh A, Nandi D, Gupta K, Chatterjee D, Ghosh UC (2015) β-Cyclodextrin modified hydrous zirconium oxide: synthesis, characterization and defluoridation performance from aqueous solution. Chem Eng J 263:220–230. https://doi.org/10.1016/j.cej.2014.11.039
37. Parashar K, Ballav N, Debnath S, Pillay K, Maity A (2017) Hydrous ZrO_2 decorated polyaniline nanofibres: synthesis, characterization and application as an efficient adsorbent for water defluoridation. J Colloid Interface Sci 508:342–358. https://doi.org/10.1016/j.jcis.2017.08.044
38. Lutfullah, Rashid M, Haseen U, Rahman N (2014) An advanced Cr(III) selective nano-composite cation exchanger: synthesis, characterization and sorption characteristics. J Ind Eng Chem 20:809–817. https://doi.org/10.1016/j.jiec.2013.06.010
39. Dhanpat R, Bruce MS, Moore DA (1987) Chromium(III) hydrolysis constants and solubility of chromium(III) hydroxide. Inorg Chem 26:345–349. https://doi.org/10.1021/ic00250a002
40. Pan X, Cheng S, Zhang C, Jiao Y, Lin X, Dong W, Qi X (2021) Mussel-inspired magnetic pullulan hydrogels for enhancing catalytic degradation of antibiotics from biomedical wastewater. Chem Eng J 409. https://doi.org/10.1016/j.cej.2020.128203
41. Qi X, Zeng Q, Tong X, Su T, Xie L, Yuan K, Xu J, Shen J (2021) Polydopamine/montmorillonite-embedded pullulan hydrogels as efficient adsorbents for removing crystal violet. J Hazard Mater. https://doi.org/10.1016/j.jhazmat.2020.123359
42. Su T, Wu L, Pan X, Zhang C, Shi M, Gao R, Qi X, Dong W (2019) Pullulan-derived nanocomposite hydrogels for wastewater remediation: synthesis and characterization. J Colloid Interface Sci 542:253–262. https://doi.org/10.1016/j.jcis.2019.02.025
43. Qi X, Liu R, Chen M, Li Z, Qin T, Qian Y, Zhao S, Liu M, Zeng Q, Shen J (2019) Removal of copper ions from water using polysaccharide-constructed hydrogels. Carbohydr Polym 209:101–110. https://doi.org/10.1016/j.carbpol.2019.01.015
44. Wu P, Zhang Q, Dai Y, Zhu N, Dang Z, Li P, Wu J, Wang X (2011) Adsorption of Cu(II), Cd(II) and Cr(III) ions from aqueous solutions on humic acid modified Ca-montmorillonite. Geoderma 164:215–219. https://doi.org/10.1016/j.geoderma.2011.06.012
45. Gomez-Gonzalez SE, Carbajal-Arizaga GG, Manriquez-Gonzalez R, De la Cruz-Hernandez W, Gomez-Salazar S (2014) Trivalent chromium removal from aqueous solutions by a sol–gel synthesized silica adsorbent functionalized with sulphonic acid groups. Mater Res Bull 59:394–404. https://doi.org/10.1016/j.materresbull.2014.07.035
46. Lesaoana M, Pakade VE, Chimuka L (2019) Crosslinker-less surface-imprinted Macadamia derived activated carbons for trace Cr(III) removal from aqueous solution. Environ Inno. https://doi.org/10.1016/j.eti.2019.100336
47. Fonseca-Correa R, Giraldo L, Moreno-Pirajáan JC (2013) Trivalent chromium removal from aqueous solution with physically and chemically modified corncob waste. J Anal Appl Pyrolysis 101:132–141. https://doi.org/10.1016/j.jaap.2013.01.019
48. Zhang F, Lan J, Zhao Z, Yang Y, Tan R, Song W (2012) Removal of heavy metal ions from aqueous solution using Fe_3O_4-SiO_2-poly(1,2-diaminobenzene) core-shell sub-micron particles. J Colloid Interface Sci 387:205–212. https://doi.org/10.1016/j.jcis.2012.07.066